16th World Conference on Earthquake, 16WCEE 2017

Santiago Chile, January 9th to 13th 2017

Paper N° 4858

Registration Code: S-J1461663623

CANYON TOPOGRAPHY EFFECTS ON GROUND MOTION

E. Skiada[(1)], S. Kontoe, P.J. Stafford, D.M. Potts

[(1)] *Research Student, Imperial College London, evangelia.skiada11@imperial.ac.uk*

Abstract

It is broadly known that topographic irregularities effect ground motions, with a particular enhancement of the ground response close to convex topographic features such as ridges and slope crests. Although there are many studies investigating the ground motion in the vicinity of slope crests, the response at the toe has not been studied in great detail, as the toe ground motion is normally considered to be smaller than that of the crest. However, for canyon topographies further investigation of the ground motion at the slope toe, where a more complicated response is expected due to the interaction of the canyon sides, is needed. The response of semi-circular and semi-elliptical canyons has been previously examined; but mainly focusing on valleys filled with soft materials. This paper considers a fully weathered canyon (*i.e.*, without any in-fill material) aiming to investigate the influence of a canyon's width on the surface ground motion through a parametric time-domain finite element (FE) study. A two-dimensional plane-strain model of an idealised canyon is considered for vertically propagating SV waves, using wavelets as input excitation. The model consists of two step-like slopes with slope height (H), in a homogeneous linear elastic soil layer overlying rigid bedrock. The analyses focus first on the canyon slope areas, where the ground motion is altered depending upon the proximity to the topographic irregularity, identifying the main parameters that effect the response. Results are also presented for several points along the canyon ground surface showing that the distribution of topographic aggravation varies significantly with canyon width.

Keywords: topography; 2D wave propagation; amplification; canyon; ground motion

1. Introduction

The substantial effect of surface topography on earthquake ground motion is well-known; especially that associated with convex areas at the ground surface during destructive earthquakes. Observations from past events, *e.g.*, Northridge 1994, Athens 1999, Haiti 2010 and Christchurch 2011, and numerical studies have shown that seismic ground motion is mainly amplified around hills, ridges and at the crests of slopes. The majority of previous numerical studies consider topographic irregularity as an isolated feature in a homogeneous half space and usually obtain amplification factors smaller than those from field observations – typically 2-3 times the free-field motion [1] – compared with amplification magnitudes ranging from 2 to 10 and reaching values up to 30 times reported in the literature [2]. Lack of numerical model complexity, presence of subsurface soil layering, use of unrealistically simplified ground motions, topographic and soil amplification interaction have been identified as possible reasons for these discrepancies.

Several studies on topographic effects have focused on the ground response around slopes, examining different soil properties and slope configurations. In particular, attention has been given to topographic effects around step-like slopes over an elastic half-space with SV input waves [3] and their dependence on the slope geometry, the predominant frequency and the duration of the input motion [4]. Ground motion incidence angle and soil stratigraphy have also been investigated as parameters effecting the response around the crest of a single slope [5, 6]. Focusing mainly on canyon slopes and especially at the crest areas, the impact of canyon topography on surface ground motion was examined for semi-cylindrical and semi-elliptical canyon shapes [7, 8]. Previous studies have indicated that the response at the canyon ground surface is effected by the canyon width in relation to the input motion characteristics [5, 7, 8]. Based on these conclusions, this paper investigates the ground response as a function of the canyon width for a range of input motion frequencies.

2. Methodology

Two-dimensional time-domain finite element analyses were performed, considering a canyon in a soil layer over rigid bedrock subjected to vertically propagating in-plane shear (SV) waves. The soil is treated as a homogeneous linearly elastic material, with properties listed in Table 1. The finite element (FE) model geometry consists of a canyon of height (H), slope inclination angle (i) and soil layer thickness (z), as presented in Fig.1. Parametric analyses focus on the impact of the normalised wavelength (H/λ) on the response by varying both the input motion wavelength (λ) and the crest-to-crest distance (L_{ctc}) of the two slopes forming the canyon sides. The distance of the crest from the lateral mesh boundary (L=500m), the slope height (H=50m) and the slope inclination angle (i=90^o) were fixed for the current study. The soil layer's fundamental frequency was then varied, using different values for the bedrock depth (z) to confirm that the conclusions are also valid for deeper soil layers. The rigid bedrock assumption is considered realistic for high stiffness-contrast interfaces. The assumed boundary condition corresponds to an impedance ratio (defined as the ratio of the bedrock properties over the soil properties) equal to infinity, which results in zero transmission of energy in the bedrock and full trapping of energy in the soil domain. Based on wave propagation analysis for impedance ratio values greater than eight, the transmitted energy within the bedrock is nearly zero and most of the energy is reflected back into the soil domain, i.e. approaching the perfectly rigid bedrock assumption.

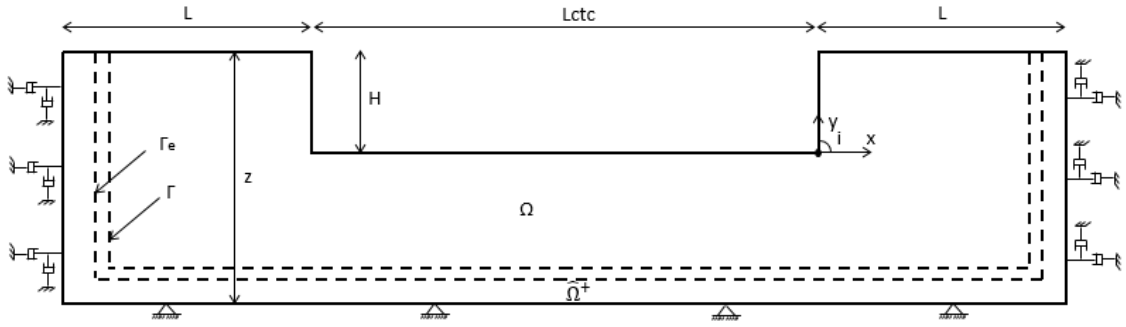

Fig. 1 – Geometry of the domain considered within the finite element analyses.

All numerical analyses were carried out with the Imperial College Finite Element Program, ICFEP [9], employing the generalised-α time integration scheme [10]. This is an unconditionally stable implicit method with second order accuracy and controllable numerical damping [11, 12]. In all analyses the time-step is taken as a fraction of the predominant period of the input motion ($\Delta t=T_p/40$). The largest element dimension, Δl, of the mesh follows the recommendation of $\Delta l \leq \lambda_{min}/10$ [13], where λ_{min} is the wavelength determined for the lowest input motion period T_p.

Concerning the location of the FE mesh boundaries, the distance of the bottom and lateral boundaries of the problem needs to be specified such that the numerical results obtained are independent of the boundary conditions. The bottom boundary location is determined based on the bedrock location. The Domain Reduction Method was used to reduce the computational domain and to ensure free-field conditions were obtained at the lateral boundaries of the FE mesh. This method is a two-step procedure for seismological applications which can be used to reduce the size of the domain to be analysed [14, 15]. During the first step (Step I), a simplified model is considered, with much smaller computational cost than analysing the whole domain. The second step (Step II) focuses on the reduced domain (area) of interest and an external region ($\widehat{\Omega}^+$). Equivalent forces calculated from the displacement field computed during Step I, are implemented as an input along the line Γ in Step II (Fig.1). The perturbation of the external area is only outgoing and corresponds to the relative response between Steps I and II. Free-field conditions can be accurately represented in the numerical model of Step II by introducing the domain reduction method together with the standard viscous boundary at the lateral boundaries [16]. In Step I of the analysis, a soil column of thickness z was used and a horizontal acceleration time-history was applied at the base of the mesh, while the vertical movement along the lateral boundaries and the base was restricted. In Step II, the standard viscous boundary was applied along the lateral boundaries and both horizontal and vertical displacements were restricted along the bottom boundary to represent the rigid bedrock assumption.

Table 1 – Considered soil parameters.

Modulus of elasticity, E	1333MPa
Mass density, ρ	2.0 Mg/m^3
Poisson's ratio, ν	1/3
Horizontal coefficient of earth pressure, K_o	1.0
Damping ratio, ξ	5% (achieved by varying Rayleigh damping parameters)

A harmonic wavelet with period T_p, modulated by Saragoni and Hart temporal filter [17] was adopted for the input motion, given by Eq. (1):

$$a(t) = \sqrt{\beta e^{-at} t^{\gamma}} \sin\left(\frac{2\pi t}{T_p}\right) \quad (1)$$

where α and γ are constants controlling the shape of the acceleration-time history, β is a constant controlling the amplitude, T_p is the predominant period of the pulse and t is time. For every considered period T_p, the values of α, β and γ were varied so as to achieve a unit amplitude of the input wavelet. The number of cycles of the input motion is kept constant and equal to 12 for all the examined input motion periods T_p. A plot of the acceleration-time history of the input motion is shown in Fig.2 for T_p=0.5sec and considered α=4, β=50 and γ=5. Acceleration time-histories at discrete points along the ground surface were obtained as the main output of the analysis. The free-field motion corresponding to the crest stratigraphy was used for the Step I column analyses (*i.e.*, the 1D model thickness for Step I was considered as z).

Topographic effects are numerically assessed by de-coupling them from the soil layer effects. To achieve this decoupling, results from the 2D seismic response analyses accounting for both topographic and soil layer amplification are compared with 1D column analysis results which represent the free-field response and account

only for the soil layer amplification. The topographic amplification factor is usually determined as the ratio of 2D to 1D (column) peak ground acceleration values or as the ratio of 2D to 1D Fourier spectra at the ground surface. For this study, the ratio of the peak horizontal ground accelerations A_h is considered in order for the amplification factors to be comparable with those of previous studies using the same definition [3, 4].

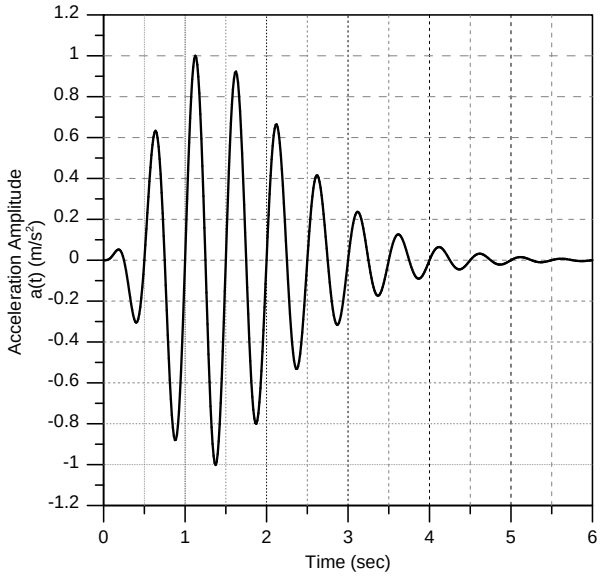

Fig. 2 – Input motion for input period T_p=0.5sec (with considered α=4, β=50 and γ=5).

3. Analysis Results

In the first set of analyses the depth to bedrock (z), the crest-to-crest distance (L_{ctc}) and the predominant input motion period (T_p) are varied in order to investigate their effect on the topographic aggravation at the ground surface. The examined frequency range is 0.1Hz to 10Hz. Table 2 summarises all the parametric analyses which include three depths to bedrock (z) and seven crest-to-crest distances (L_{ctc}). The results are presented in terms of the normalised horizontal acceleration (A_h) at the crest and the toe of the slopes. Normalised response for the crest refers to the ratio of the maximum horizontal acceleration at the crest of the slope resulting from the 2D numerical analyses to the maximum horizontal free-field acceleration, *i.e.*, acceleration of the 1D soil column with height equal to the crest height (z). Similarly, normalised response for the toe refers to the ratio of the maximum horizontal acceleration at the toe of the slope resulting from the 2D numerical analyses to the maximum horizontal acceleration of the 1D soil column with height equal to the toe height (z-H).

Table 2 – Parameters varied within the numerical model

Depth to bedrock z (m)	**Crest-to-crest distance L_{ctc} (m)**
125	20, 40, 80, 280, 520, 1000, 2000
250	280, 520, 1000
500	20, 40, 80, 280, 520, 1000

3.1 Ground motion at the crest and toe of the canyon slopes

The absolute peak horizontal acceleration conditional upon a unit amplitude input motion, was computed at several points along the ground surface, both inside and outside of the canyon. The response in terms of normalised horizontal acceleration computed at the crest (x, y)=(0,H) and the toe (x, y)=(0,0) of the slope with H/λ is presented in Figs 3 to 5, for the three considered depth to bedrock values respectively, where λ refers to the wavelength corresponding to the predominant input motion period. The normalisation of the maximum crest or toe acceleration by the corresponding free-field value allows the topographic effects on the ground surface to

be isolated from the combined topographic and soil layer aggravation. The transfer functions of 1D soil columns corresponding to the free-field soil layer examined thicknesses are also superimposed in each figure (1D elastic). These transfer functions describe the ratio of the displacement amplitudes at the top and the bottom of the uniform, damped soil layer overlying rigid bedrock. In Fig.5a, the crest response computed in this study for a depth to bedrock of z=500m, is compared to the results of Ashford *et al*. [3] and Bouckovalas & Papadimitriou [4] who analysed a slope of height H=30m within an elastic half-space (*i.e.*, infinite depth to bedrock).

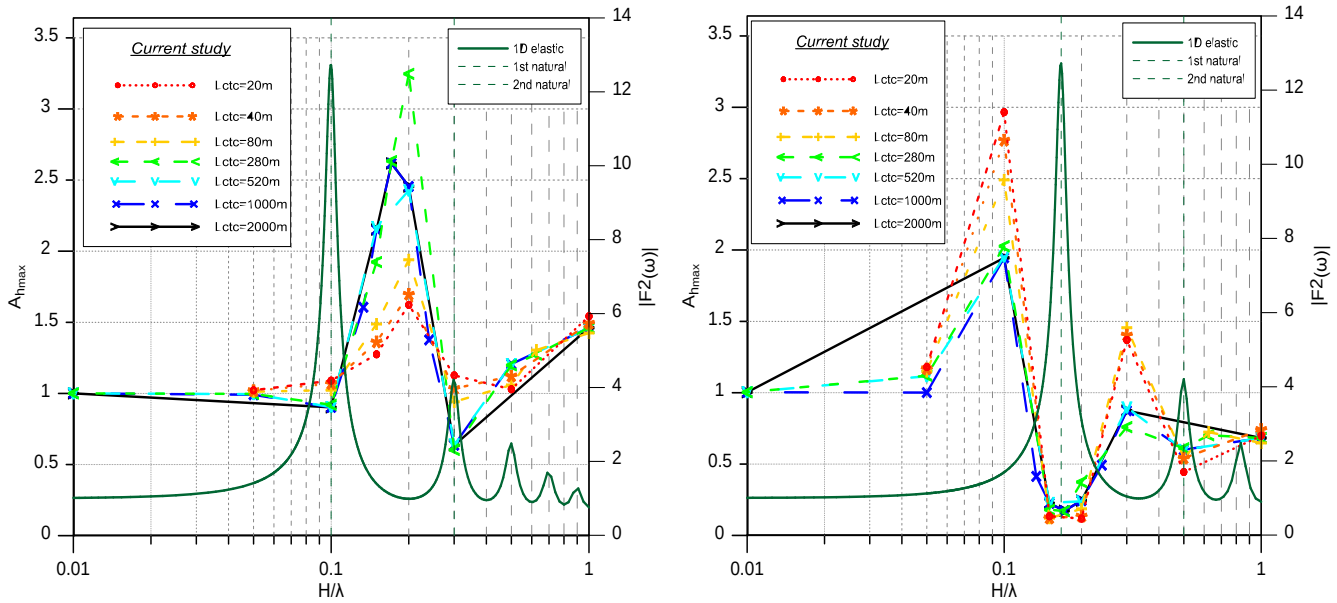

Fig. 3 – Crest (a) and toe (b) amplification response for different crest-to-crest distances for depth to bedrock z=125m.

The maximum normalised amplification for the crest of the slope occurs at H/λ=0.2 for z=125m (Fig. 3a). The maxima lie in between the first and second natural periods of the 1D crest profile (1D elastic). They occur at H/λ=0.2 mainly because the 1D crest maximum horizontal acceleration, which is used for the normalization, has a very small value at these periods. As the soil layer amplification is much smaller in that range, it is easier for the topographic amplification to be observed. The specific H/λ ratios of topographic amplification maxima correspond to the oscillation frequencies of the slopes. These frequencies depend on the slope height (H), the considered shear wave velocity (V_s), the depth to bedrock (z) and the crest-to-crest distance (L_{ctc}). The maxima occur at similar H/λ ratios, irrespective of the crest-to-crest distance variation. However, the magnitude of the amplification varies for the different examined canyon widths, with the largest occurring for L_{ctc}=280m. The high amplification for this scenario can be explained by the fact that the corresponding input wavelength of λ=250m for H/λ=0.2, is comparable to the canyon width, and the canyon appears to resonate with the input motion in this case. This confirms the observation that canyon response maximizes for input motion wavelengths comparable to the canyon dimensions [7, 8].

Maximum normalised amplification at the toe of the slope occurs at H/λ=0.1 for all the examined crest-to-crest distances. This input motion frequency corresponds to the first natural frequency of the crest thus the toe response seems to be mainly affected by the crest resonance. The amplitudes of the maxima observed at the toe become larger for smaller values of the crest-to-crest distance. This arises because for narrower canyon geometries, the toe area is mainly effected by the interaction of the canyon sides. In Fig. 3b it is seen that the interaction of the canyon slopes is greater for canyon widths up to 80m. For larger canyon widths the toe normalised maxima remain almost the same for all the examined input motion frequencies.

Fig.4 and Fig.5 depict the response at the slope crest and toe points for the intermediate (z=250m) and the largest (z=500m) examined depths to bedrock, respectively. The maxima for the crest occur at ratios of H/λ

equal to 0.1 and 0.2 for z=250m (Fig. 4a) and H/λ=0.2 for z=500m (Fig.5a). Similar to the smallest depth to bedrock case (z=125m), the maxima for z=250m lie in between the first and second natural periods of the crest (1D elastic). The maxima locations do not shift with varying canyon widths, however the amplification values change with crest-to-crest distance. Although only a small number of canyon widths have been examined for the intermediate depth to bedrock case, the largest maximum occurs for L_{ctc}=520m as expected. The examined canyon width in this case is comparable to the input motion wavelength of λ=500m for case of H/λ=0.1. For the intermediate depth to bedrock case, the maximum toe response occurs at H/λ ratios corresponding to the first natural frequency of the crest, as in the shallow depth to bedrock case (H/λ=0.05 for 250m). Similarly, the toe maxima values increase for narrower canyon cases. For the deepest soil layer case, the slope height is very small compared to the crest and toe heights which are similar, and therefore the slope response maximizes at an H/λ ratio much larger than the ratios corresponding to the fundamental frequencies of the crest and the toe.

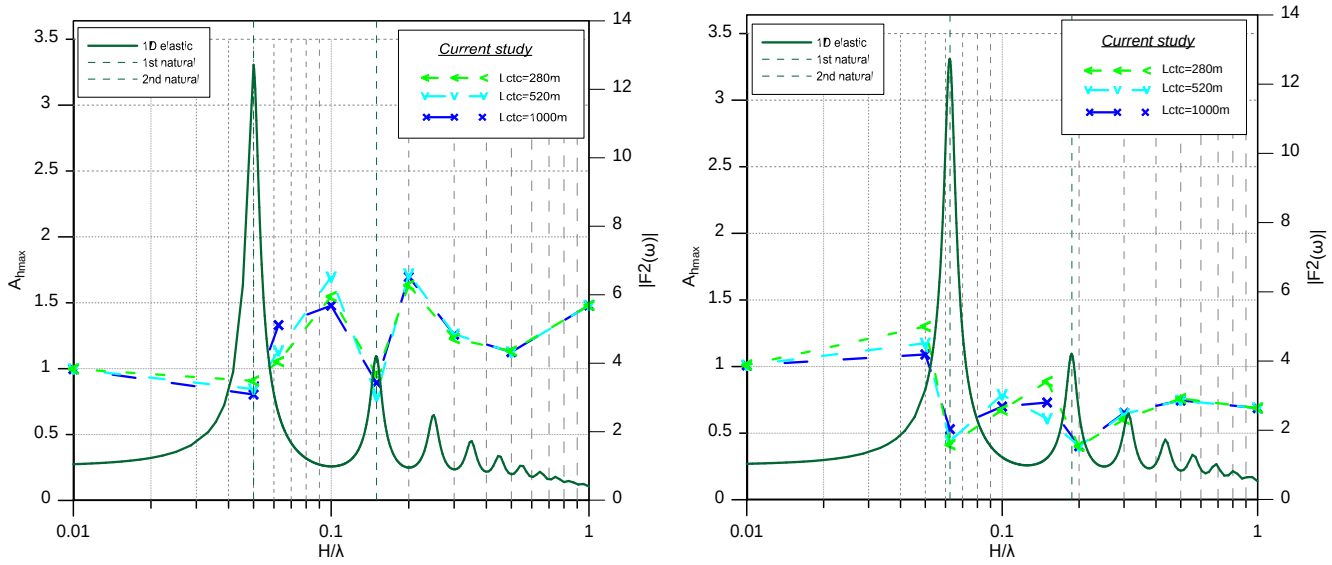

(a) (b)

Fig. 4 – Crest (a) and toe (b) amplification response for different crest-to-crest distances for depth to bedrock z=250m.

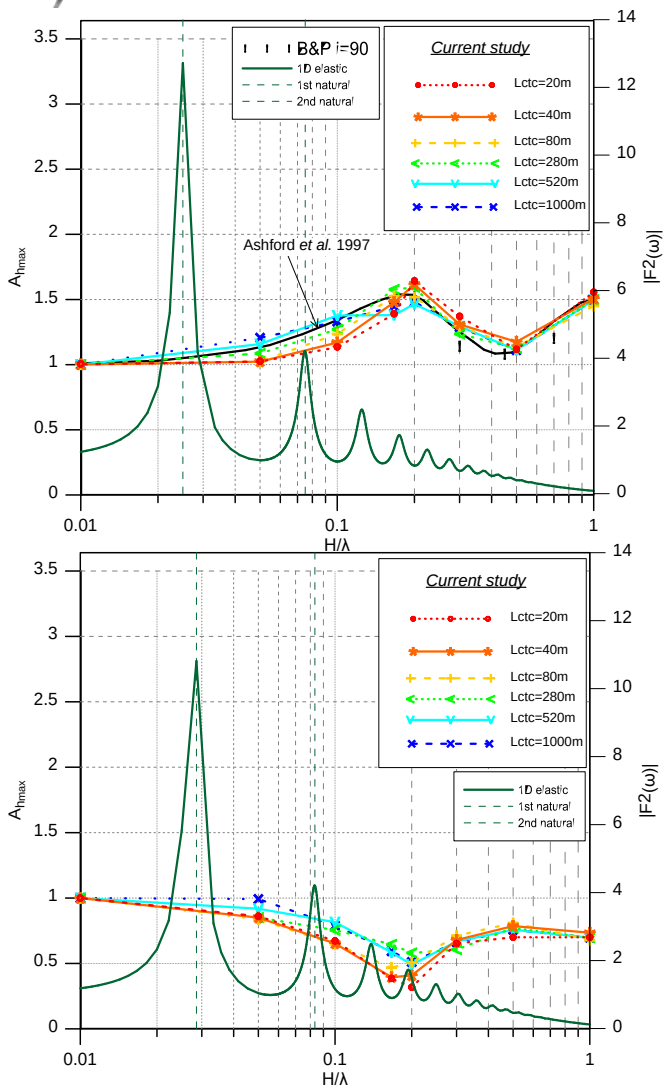

(a) (b)

Fig. 5 – Crest (a) and toe (b) amplification response for different crest-to-crest distances for depth to bedrock z=500m.

The amplification magnitude depends on the depth to bedrock (z) value and increases with decreasing depth to bedrock due to the stiff interface being closer to the ground surface. The case of z=500m approaches the response of the half-space case as seen from the comparison with the results from the literature (Fig.5a). The oscillation mechanism of the slope depends on the considered depth to bedrock (z) in comparison to the slope height (H). The effect of the depth to bedrock parameter on the surface ground response for a single slope has been discussed in detail by [18]. The crest-to-crest distance variation does not significantly affect amplification for the z=500m case because the topographic irregularity is small compared to the soil layer thickness.

3.2 Ground motion at several points on the canyon surface

For the results presented above, the overall maximum normalised acceleration response is observed for the shallowest depth to bedrock case of z=125m and for a crest-to-crest distance value of L_{ctc}=280m. In this section, only this shallow depth to bedrock case is considered. The focus now is upon the variation of the maximum horizontal aggravation A_h with normalised distance from the centre of the canyon for several points at the ground surface, both inside and outside the canyon (Fig.6). This case refers to the overall maximum normalised

amplification observed for H/λ=0.2 for the crest point, which corresponds to an input motion with a period T_p=0.5sec.

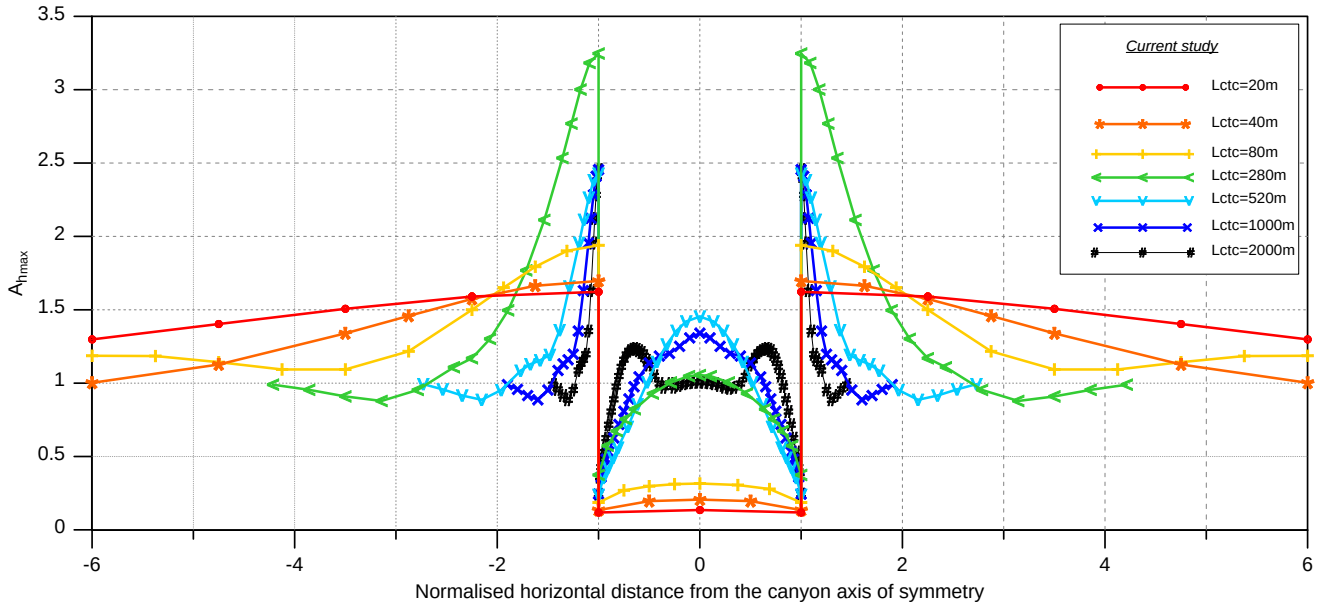

Fig. 6 – Maximum horizontal aggravation A_h with normalised distance from the canyon axis of symmetry for several points on the ground surface for input motion period T_p=0.5sec (H/λ=0.2) and z=125m.

As previously discussed, when the input motion wavelength coincides with the canyon width, response at the crest and the toe of the canyon slopes maximises. As seen in Fig.6, the maximum on the slope itself is observed for L_{ctc}=280m for both the crest and the toe. The response decreases towards the free-field response for the points behind the crest. Canyons with crest-to-crest distances equal or larger than the input motion wavelength are mainly affected. For the points in the canyon, the response maximises at the centre for all the canyon widths except the largest examined one (L_{ctc}=2000m). This occurs due to the interaction of the canyon sides at this specific input motion frequency. For specific input motion wavelengths, comparable and larger than the canyon width, the maximum at the canyon centre becomes even larger. This happens both due to the interaction between the slopes and the canyon oscillation with the input motion period. Finally, for L_{ctc}=2000m, although response at the crest is similar to the other examined values of the canyon width, the response in the canyon differs. This is because as the canyon sides are too far apart, there is no interaction between them and the change in the ground motion is only observed close to the topographic irregularity for this specific input motion frequency.

4. Conclusions

For the crest of the slope, amplification maxima locations depend on the slope oscillation and its characteristics – *i.e.*, slope height and shear wave velocity. Amplification maxima occur at H/λ ratios intermediate to those corresponding to the fundamental periods of the 1D crest response. Since the slope characteristics were not altered during the parametric analyses of this study, amplification maxima locations do not change with varying the crest-to-crest distance. However, the magnitude of maximum amplification changes and is larger for the canyon width corresponding to the input motion wavelength. Response at the toe of the slope is mainly affected by the crest oscillation, thus it maximizes for H/λ ratios corresponding to the fundamental ratios of the 1D crest. The amplification magnitude becomes larger for smaller canyon widths, because of the proximity of the two canyon slopes and their interaction. The depth to bedrock parameter controls only the value of the maximum amplification which is larger for smaller depth to bedrock values.

For all the points on the ground surface of the canyon, either back from the crest or inside the canyon, the response is controlled by both the interaction of the slope sides and the canyon width. Especially when the

canyon width coincides with the input motion wavelength, response at the canyon crest and toe maximizes. For the specific input motion wavelength that was presented herein, a maximum is observed at the canyon centre for a range of canyon widths and not only for the case where the width coincides with the input motion wavelength. For very wide canyons, the canyon centre is further away from the topographic irregularity and is not affected. The maximum response in that case is observed near the canyon sides, close to the topographic irregularity.

5. Acknowledgements

The first author would like to gratefully acknowledge the financial support by the Imperial College PhD Scholarships Programme.

6. References

[1] Pedersen H, Le Brun B, Hatfield D, Campillo M, Bard P-Y (1994): Ground motion amplitude across ridges. *Bulletin of the Seismological Society of America*, **84** (6), 1786-1800.

[2] Geli L, Bard P-Y, Jullien B (1988): The effect of topography on earthquake ground motion: a review and new results. *Bulletin of the Seismological Society of America*, **78** (1), 42-63.

[3] Ashford SA, Sitar N, Lysmer J, Deng N (1997): Topographic effects on the seismic response of steep slopes. *Bulletin of the Seismological Society of America*, **87** (3), 701–9.

[4] Bouckovalas GD, Papadimitriou AG (2005): Numerical evaluation of slope topography effects on seismic ground motion. *Soil Dynamics and Earthquake Engineering*, **25**, 547–58.

[5] Assimaki D, Gazetas G (2004): Soil and topographic amplification on canyon banks and the 1999 Athens earthquake. *Journal of Earthquake Engineering*, **8** (1), 1-43.

[6] Assimaki D, Kausel E, Gazetas G (2005): Wave propagation and soil–structure interaction on a cliff crest during the 1999 Athens Earthquake. *Soil Dynamics and Earthquake Engineering*, **25**, 513–527.

[7] Trifunac MD (1973): Scattering of plane SH waves by a semi-cylindrical canyon. *International Journal of Earthquake Engineering and Structural Dynamics*, **1**, 267-281.

[8] Wong HL, Trifunac MD (1974): Surface motion of a semi-elliptical alluvial valley for incident plane SH waves. *Bulletin of the Seismological Society of America*, **64** (5), 1389-1408.

[9] Potts DM, Zdravković L (1999): *Finite element analysis in geotechnical engineering*. Thomas Telford.

[10] Chung J, Hulbert GM (1993): A time integration algorithm for structural dynamics with improved numerical dissipation: the generalized-a method. *Journal of Applied Mechanics*, **60,** 371–5.

[11] Kontoe S, Zdravković L, Potts DM (2008): An assessment of time integration schemes for dynamic geotechnical problems. *Computers and Geotechnics*, **35** (2), 253–64, http://dx.doi.org/10.1016/j.compgeo.2007.05.001.

[12] Kontoe S, Zdravković L, Potts DM (2008): The domain reduction method for dynamic coupled consolidation problems in geotechnical engineering. *International Journal for Numerical and Analytical Methods in Geomechanics*, **32** (6), 659–80.

[13] Kuhlemeyer RL, Lysmer J (1973): Finite element method accuracy for wave propagation problems. Technical note. *Journal of Soil Mechanics and Foundation Division*, **99** (5), 421–7.

[14] Bielak J, Loukakis K, Hisada Y, Yoshimura C (2003): Domain reduction method for three-dimensional earthquake modelling in localized regions. Part I: theory. *Bulletin of the Seismological Society of America*, **93** (2), 817–824.

[15] Kontoe S, Zdravković L, Potts DM (2009): An assessment of the domain reduction method as an advanced boundary condition and some pitfalls in the use of conventional absorbing boundaries. *International Journal for Numerical and Analytical Methods in Geomechanics*, **33**, 309–30.

[16] Lysmer J, Kuhlemeyer RL (1969): Finite dynamic model for infinite media. *Journal of the Engineering Mechanics Division*, ASCE, **95** (4), 859–77.

[17] Saragoni GR, Hart GC (1974): Simulation of Artificial Earthquakes. *Earthquake Engineering and Structural Dynamics*, **2**, 249-267.

[18] Tripe R, Kontoe S, Wong TKC (2013): Slope topography effects on ground motion in the presence of deep soil layers. *Soil Dynamics and Earthquake Engineering*, **50**, 72-84.